Ocean Engineering 343 (2026) 123330

Contents lists available at ScienceDirect

Ocean Engineering

journal homepage: www.elsevier.com/locate/oceaneng

Research paper

Surface-laid pipelines and cables in areas of sand waves and seabed mobility: quantitative analysis from a decade of field observations

Zhechen Hou [a,*], Fraser Bransby [a], David White [b], Phillip Watson [a], Andrew Rathbone [c], Han Eng Low [d]

[a] Centre for Offshore Foundation Systems (COFS), Oceans Institute, School of Earth and Oceans, The University of Western Australia, Perth, Australia
[b] School of Engineering, The University of Southampton, Southampton, UK
[c] Wood Australia, Perth, Australia
[d] Fugro Australia Pty Ltd, Perth, Australia

ARTICLE INFO

Keywords:
Pipelines
As-laid embedment
Temporal changes
Mobile seabeds
Sand waves
Free-spans
On-bottom stability
Scour onset

ABSTRACT

The embedment and spanning of surface-laid offshore pipelines and cables can change during their operational life due to seabed mobility. Understanding these changes is important as it affects their operational response. However, systematic interpretation of long-term observation data across different projects and in different seabed environments is lacking.

This study analyses the survey data of three different pipelines with diameters ranging from 4 to 42 inches, installed in two different sand wave fields on the Northwest Shelf of Australia. These surveys were carried out from the as-laid (initial) condition to a maximum period of 13 years after installation. The results quantify how the proportion of the pipeline length that is in span reduces over time, and identifies approximately 2- to 3-fold embedment increases in certain parts of the sand waves. Notably, the data reveals that current design practice significantly underestimates as-laid embedment by a factor of approximately ten and that temporal changes are not usually considered.

Quantitative insights due to these changes were further assessed, including geotechnical aspects, structural aspects, hydrodynamic loading and stability, and the progression of scour. These findings illustrate the value of a multi-disciplinary approach to evaluate the long-term integrity of cables and pipelines.

1. Introduction

1.1. Background

Subsea pipelines and cables are used to transport energy offshore in both the renewables and oil and gas industries. For example, the total length of offshore pipelines in Australia exceeds ~6500 km (Australian Government, 2025) – with an industry value of $20 billion and a typical through-life cost of $3 million/km. Meanwhile, the subsea power cable network worldwide is on the order of millions of kilometres (Ardelean and Minnebo, 2015) and is growing rapidly with the development of offshore renewable energy and the interconnection of national electricity grids. Pipelines and cables are typically laid on the seabed, but may be buried for protection. The ability of on-bottom pipelines and cables to deal with loading from internal pressure and temperature, or hydrodynamic action depends on the seabed reaction forces as they move laterally and axially on the seabed (Bruschi et al., 1997; Randolph and White, 2008a; Cheng et al., 2009; White et al., 2014, 2015a; Bransby et al., 2020). These seabed reaction forces depend strongly on the level of embedment, which must therefore be well understood to ensure the integrity of pipelines and cables. The performance and operational range of subsea power cables depends on the thermal environment, which is also affected by the level of embedment (Dix et al., 2017; Unsworth et al., 2023).

1.2. As-laid embedment

The embedment immediately after installation (i.e., 'as-laid' embedment as shown in Fig. 1a) is the starting point in geotechnical pipeline-soil interaction (PSI) calculations (the term pipeline-soil interaction is used, but applies equally to cable-seabed interaction). However, prediction of as-laid embedment includes significant uncertainty

* Corresponding author.
E-mail address: zhechen.hou@uwa.edu.au (Z. Hou).

https://doi.org/10.1016/j.oceaneng.2025.123330
Received 7 July 2025; Received in revised form 27 September 2025; Accepted 26 October 2025
Available online 10 November 2025

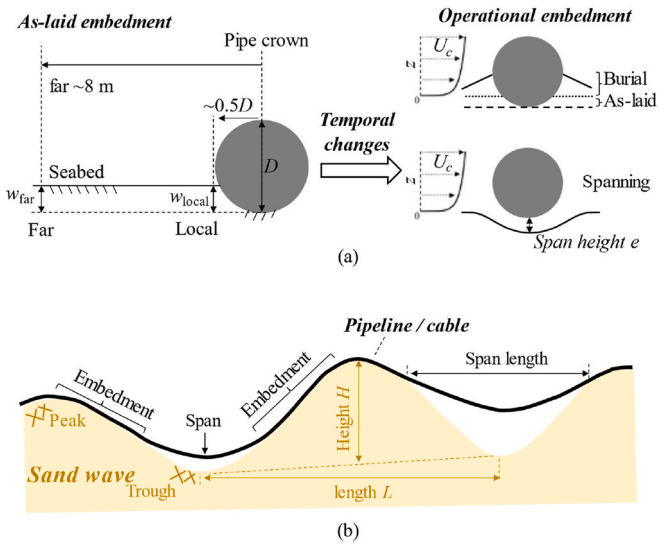

Fig. 1. (a) Embedment definition and its potential temporal changes (b) Schematic drawing of pipeline and cable on sand waves (note: vertical scale exaggerated).

because of the dynamic lay process and seabed variability (Randolph and White, 2008b; Westgate et al., 2010; Bransby et al., 2020). This uncertainty is especially significant in transitional soils with uncertain drainage conditions during laying, and in carbonate soils, which have high friction angles, wide grain size distribution, large compression ratio and reduced cyclic strength (Watson et al., 2019; Bransby et al., 2020). For example, Hou et al. (2023a) showed that the use of recommended practice approaches (DNV AS, 2021a) leads to significant under-estimation of pipeline as-laid embedment and that approximately 10-times less stiff soil springs are required to match field observations.

1.3. Temporal changes of embedment

Pipeline embedments may continually change with time after installation (see Fig. 1a) due to sediment mobility effects including (i) scour that erodes the surrounding soil away, and (ii) sedimentation that increases local embedment (e.g. Sumer et al., 2001; Bransby et al., 2014; Leckie et al., 2015; Zhang et al., 2023). Scour can create and alter free spans, which requires fatigue risk assessment.

Current design guidance (e.g. DNV AS, 2021a,b,c,d and e) only considers embedment or spanning changes if they threaten pipeline integrity. For example, longer spans and changes in burial condition may reduce the reliability (and tolerability) of a pipeline thermal management scheme, or may cause a cable or pipeline to be less stable under hydrodynamic action (Sumer and Fredsøe, 1994; Palmer, 1996; White et al., 2015; Leckie et al., 2018). Predicting future as-laid spanning helps to assess the need for costly pre-lay intervention, e.g., adding or removing seabed material to alter the local bathymetry. However, confidence in predicting temporal changes remains low. Consequently, spans are managed via costly inspections and follow-up interventions throughout the operating life (e.g. Peek and Kristiansen, 2009; Madeley et al., 2015; Low et al., 2018).

Temporal changes in embedment may be beneficial if they reduce spans and increase embedment, reducing fatigue and increasing hydrodynamic stability (Bransby et al., 2014; Rodriguez et al., 2014; White et al., 2015b; Leckie et al., 2016a, 2016b; Hou et al., 2023b). However, current practice does not generally rely on these improvements due to uncertainty in predicting through-life changes in embedment.

1.4. Embedment in sand wave areas

The aforementioned uncertainties are further exacerbated for pipelines and cables laid over bedforms, e.g., ripples, mega-ripples and sand waves with different wave lengths and heights (Allen, 1980; Matthieu and Raaijmakers, 2013; Roetert et al., 2017; Huang et al., 2020; Adnyani et al., 2023). Accurate prediction of as-laid embedment and initial spanning is hampered by uncertainty in both the bedform configurations (shown schematically in Fig. 1b) and the soil conditions (Bransby et al., 2010; Van den Abeele and Denis, 2012; Hou et al., 2023a). Furthermore, the temporal changes of pipeline and cable embedment in sand wave areas, and the resulting impact on integrity, has not been previously investigated in detail.

1.5. Current research

Many prior studies have investigated as-laid embedment and subsequent temporal changes, via experimental testing in geotechnical centrifuges (Cheuk and White, 2011; Westgate et al., 2013), mobile bed tests in O-tube flumes (An et al., 2013; Leckie et al., 2018) and field data analysis (Westgate et al., 2009; Leckie et al., 2015). The research based on field data has generally been limited to single projects and thus is hard to generalize (Leckie et al., 2016).

In the present work, extensive data sets from multiple years of observations across different projects have been collated (Hou et al., 2023b), providing the opportunity for new insight. This paper presents data from more than ten years of observations of pipelines ranging from 4 to 42 inches in diameter and laid across dormant sand waves composed of a range of carbonate sediments. The as-laid embedment is presented first, with the evolution of embedment and free-spanning with time then analysed. The findings provide quantitative data on how the burial and spanning condition of surface-laid pipelines and cables in sand wave areas varies through their operating life.

2. Field data types

2.1. Pipeline properties

The properties of the three pipelines in this study are summarised in Table 1. They cover a tenfold range of diameters and vary in bending

Table 1
Properties of the three selected pipelines.

Description	Parameter	Pipeline A: Trunkline	Pipeline B: Flowline	Pipeline C: MEG line
Outer diameter	D: mm	1159	640	105.6
Steel outer diameter	D_s: mm	1069	508	101.6
Steel wall thickness	t: mm	29.6	23.1	7.6
Insulation coating thickness	mm	6	26	2
Concrete coating thickness	mm	40	40	–
Bending stiffness	EI: MNm^2	2720.2	214.6	0.52
As-laid weight	W'_{lay}: kN/m	1.2	2.1	0.09
Flooded weight	$W'_{flooded}$: kN/m	9.2	3.7	0.149
Operational weight[a]	W'_{op}: kN/m	2.8	2.4	0.154
Specific gravity	SG, as-laid	1.1	1.6	2
	SG, flooded	1.9	2.2	2.7
	SG, operating	1.3	1.7	2.8
Lay tension	T_0: kN	900	284	–

[a] The assumed gas mixture density is 200 kg/m^3 and assumed MEG density is 1113 kg/m^3.

stiffness by a factor of 5,000. All three pipelines were laid empty and subsequently flooded, before being brought to operational conditions. The submerged weight changed significantly across these conditions, with the greatest difference being a ratio of $W'_{flooded}/W'_{lay} \approx 8$ for Pipeline A. Fig. 2 shows the alignment of representative 2-km sections of each pipeline overlain on the bathymetry. Pipeline A crosses 'sand wave area 1 (Area 1)' (Fig. 2a) while Pipelines B and C traverse the same 'sand wave area 2 (Area 2)' (Fig. 2b) but are parallel and ~100 m apart.

2.2. Sand waves

The lengths and heights of the sand waves (as defined in Fig. 1b) are summarised in Fig. 3. The orientation of the pipeline axis compared to the sand wave ridge lines was also considered for potential correction of sand wave length. The sand wave heights in both areas are lower than the ranges in a previously-published database (Flemming, 1988), but are consistent with another sand wave area ('Broome type 1') elsewhere on the Northwest Shelf of Australia (Lebrec et al., 2022). Area 1 covers ~15 km of the Pipeline A route, while Area 2 covers ~5 km of the routes of Pipelines B and C. In Area 2 the sand waves are approximately double the length and triple the height of those in Area 1, indicating greater steepness (H/L).

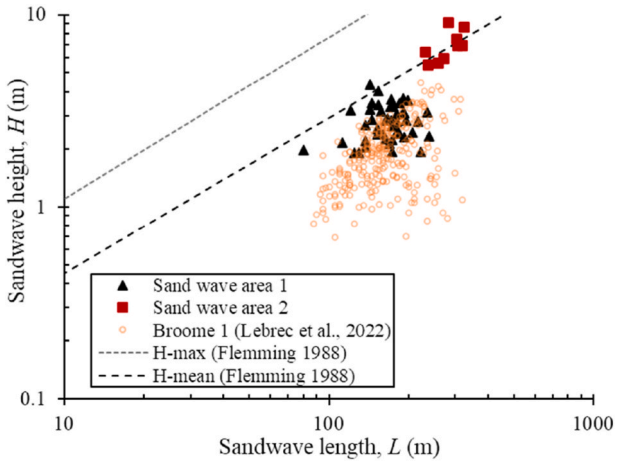

Fig. 3. Summary of sand wave characteristics in both sand wave areas.

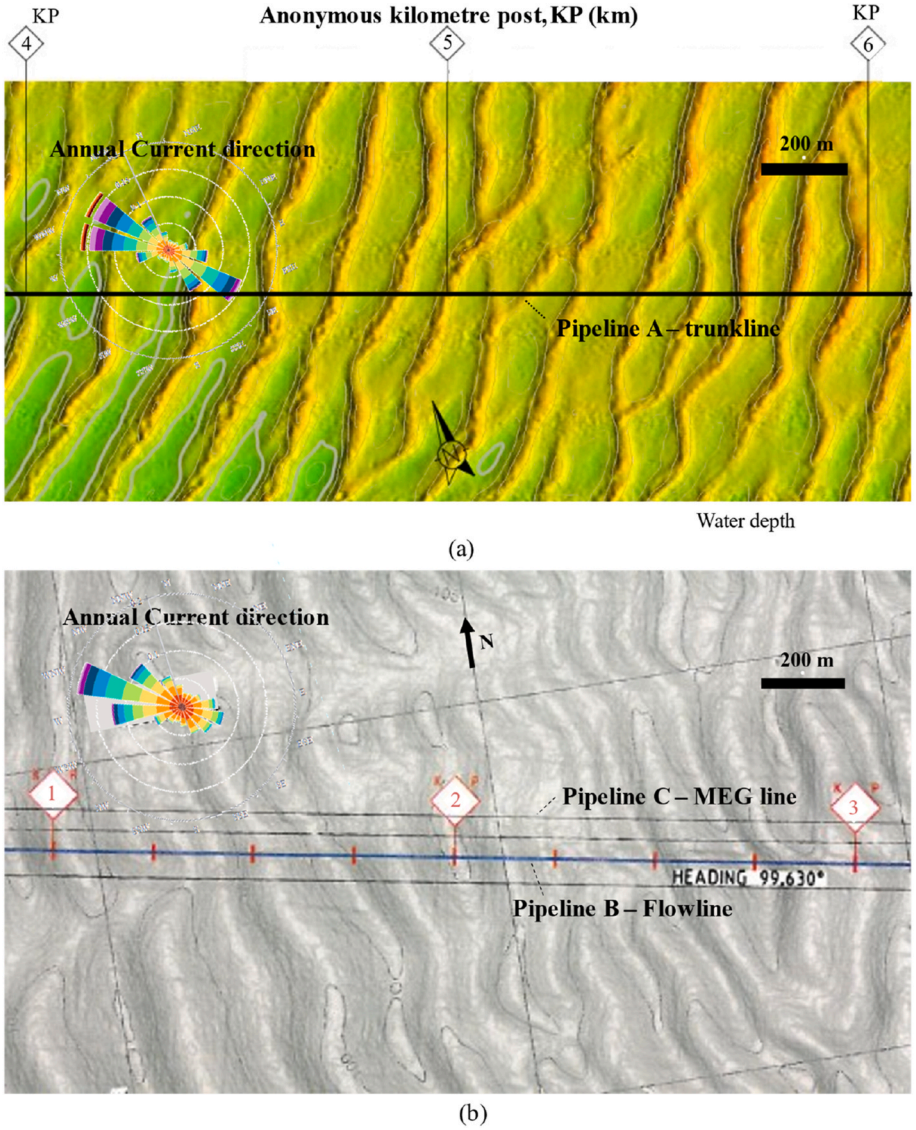

Fig. 2. Bathymetry information with anonymous kilometer post (KP): (a) Sand wave area 1 (Pipeline A); (b) Sand wave area 2 (Pipeline B and Pipeline C).

2.3. Seabed properties

Geotechnical site investigation data from boreholes and cone penetration tests (CPTs) in both sand wave fields indicate seabed materials ranging from fine carbonate silts to coarse carbonate sands. The cone penetration resistance, q_c, for the top 1 m of the seabed and the associated particle size distribution (PSD) curves are shown in Fig. 4a and b, respectively. The measured q_c in Area 1 is about 10 times lower than Area 2. This is consistent with the PSD results where the seabed materials in Area 1 consist of carbonate sandy silt to silty sand conditions (i.e., fines content range from 62 % to 95 %), and Area 2 is predominantly coarser 'clean' carbonate sand (i.e., fines content range from 3 % to 21 %). Other soil properties are summarised in Table 2, based on the geotechnical interpretative reports.

2.4. Metocean conditions

A statistical summary of the current at 1 m above seabed level in the middle of Area 1 shows that the dominant current directions are North-West (NW) to West-North-West (WNW) and South-East (SE). These currents are approximately equal, being tidal-driven, but slightly weaker towards the SE. In Area 2, the current at 1 m above seabed is predominantly in the NW to W direction with a lower occurrence in the opposite direction. The 0.01 % exceedance values of the maximum current speed at 1 m above seabed (ASB) are 0.71 m/s and 0.62 m/s for Areas 1 and 2 respectively. The orientation of the current to each pipeline is illustrated on Fig. 2.

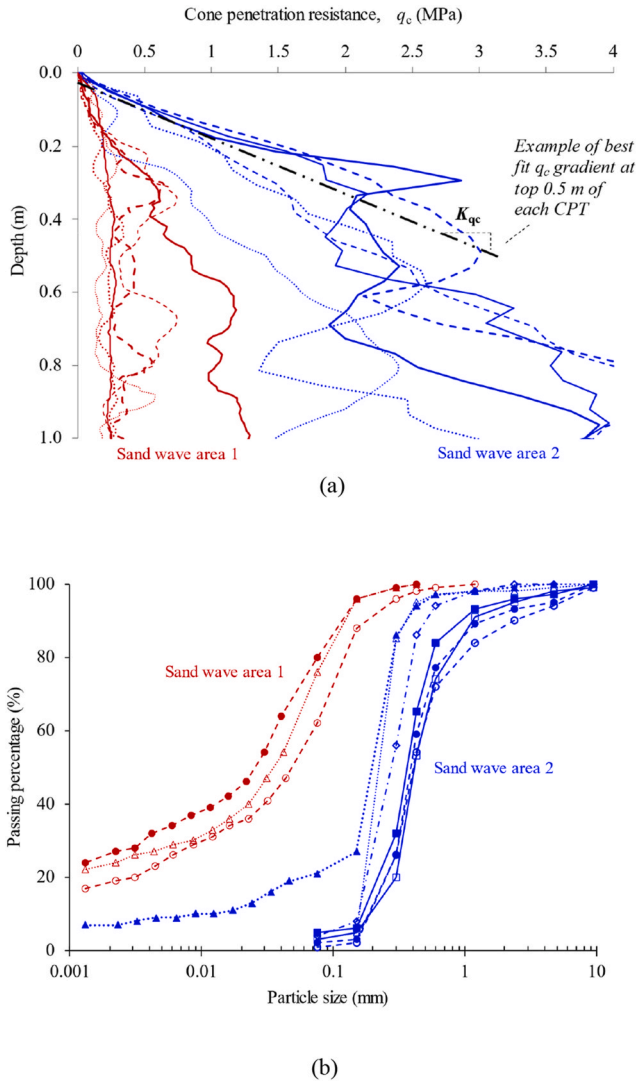

Fig. 4. (a) Cone tip penetration resistance profiles and (b) Particle size distribution (PSD) curves for sand wave area 1 (pipeline A) and sand wave area 2 (pipelines B and C).

Table 2
Soil and current properties in two sand wave areas.

Description	Parameter	Sand wave area 1	Sand wave area 2
Effective unit weight	γ': kN/m^3	5.6–8	10.5–11.7
Carbonate content	CO_3 (%)	86–98.3	93.6–98.9
Median particle size	D_{50}: mm	0.035–0.048	0.21–0.42
Fines content	% (<75 μm)	62–95	3–21
Clay-sized content	% (<2 μm)	18.6–58.7	<5
Specific gravity	G_s	2.76–2.82	2.80–2.84
Water content	w_c (%)	46.2–80.6	18.3–26.1
Internal friction angle	Φ'	38–56	39–48
Porosity	n	0.56–0.69	0.38
Current velocity (1 m above seabed)	U_{max} (m/s)	0.71	0.62

2.5. Pipeline survey data

The pipeline surveys measure the water depth at the pipe crown position (see Fig. 1a), as well as the 'local' and 'far' positions corresponding to different lateral offsets from the pipeline's springline. This allows the average local and average far embedments of the pipeline (from measurements at both sides of the crown position) to be calculated – noting that for pipelines in sand wave areas, free-spanning in the troughs may also occur. These data are measured at intervals of 0.5–1.0 m along the pipeline routes.

3. Results

3.1. As-laid embedment (example pipeline sections)

Fig. 5 shows the typical configuration for 800-m sections of each pipeline based on the first survey. For Pipelines A and B, the presented configurations represent the 'as-laid' condition (i.e., for negligible time after pipeline installation), while for Pipeline C the first survey data was after six years. For each pipeline there are two sub-figures – the left (Fig. 5a, c and 5e) show three-dimensional profiles of the seabed and pipeline geometry, while the right (Fig. 5b, d and 5f) show the along-pipe profiles of local and far embedment (as well as water depth on the secondary axis). Moving averages of pipeline embedment, calculated over 25 m lengths, are also shown, with negative values of embedment representing regions of free span.

For the large diameter and high stiffness Pipeline A, significant spans are observed over the sand wave troughs – with span lengths of up to 155 m long, and maximum gap heights of 0.6–1.6 m close to the trough of each sand wave. The embedded sections ('span shoulders') on the sand wave peaks are generally short (in the range of 20–40 m) with typical maximum local embedment of ~0.2 D. The local embedment is slightly greater than the far embedment, indicating some mounding of soil adjacent to the pipeline. Note that the somewhat lower local embedment at around KP 5.15 and 5.3 (see Fig. 5b) is due to a lateral trench created by pre-lay intervention on the associated sand wave peaks.

In contrast, the more flexible Pipeline B – which has ten times lower EI compared to Pipeline A – shows generally continuous contact with the seabed in the sand wave area, where the embedment ratio (i.e. w/D) is 0.1–0.2. No significant spans are observed, despite the higher average steepness of the sand waves in Area 2 (with H/L~0.025) compared to those in Area 1 where the trunkline is located (H/L~0.017).

The first survey of the flexible Pipeline C at $t = 6$ years also shows

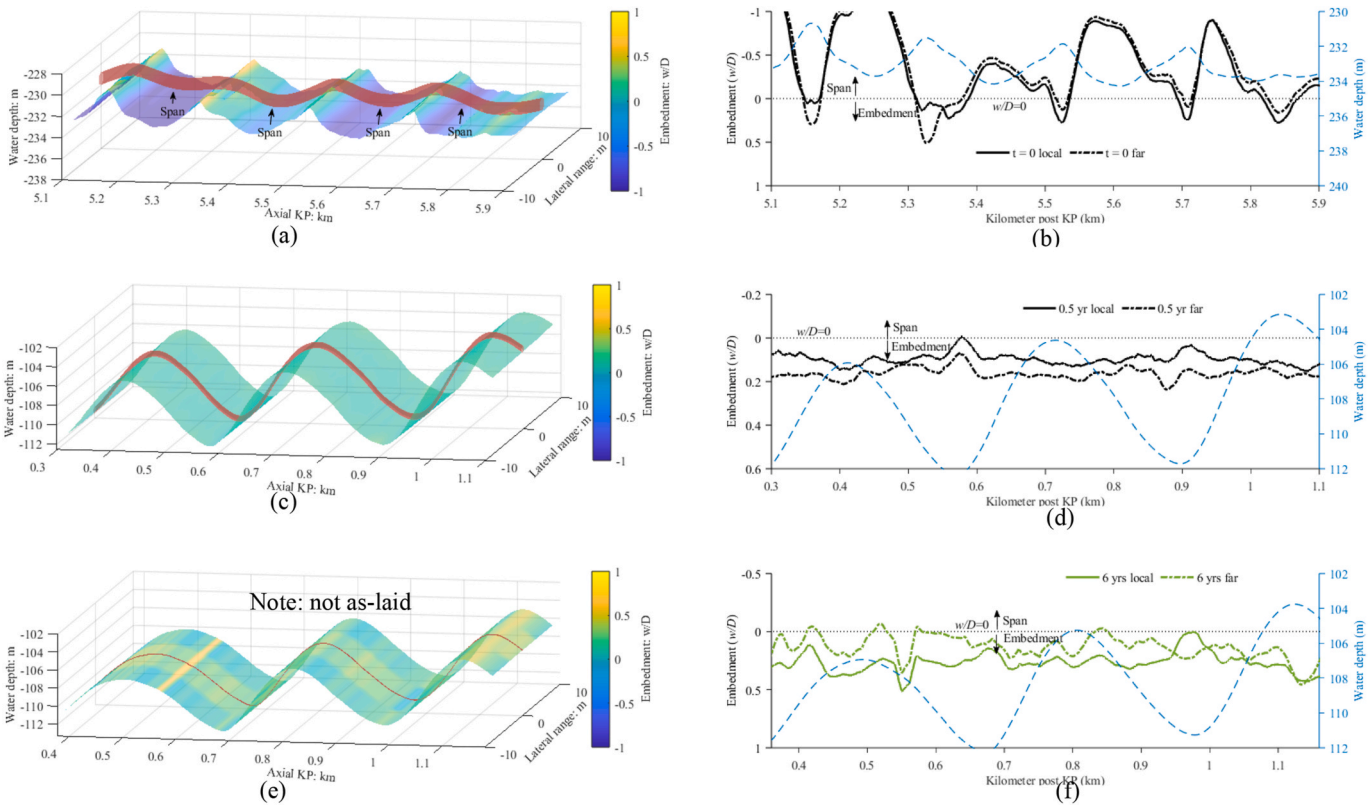

Fig. 5. Embedment from first survey (a) Pipeline A: at t = 0 (b) Pipeline A: embedment profile at t = 0 (c) Pipeline B – 3D contour at t = 0.5 year (d) Pipeline B – embedment profile at t = 0.5 year (e) Pipeline C – 3D contour at t = 6 years (f) Pipeline C – embedment at t = 6 years.

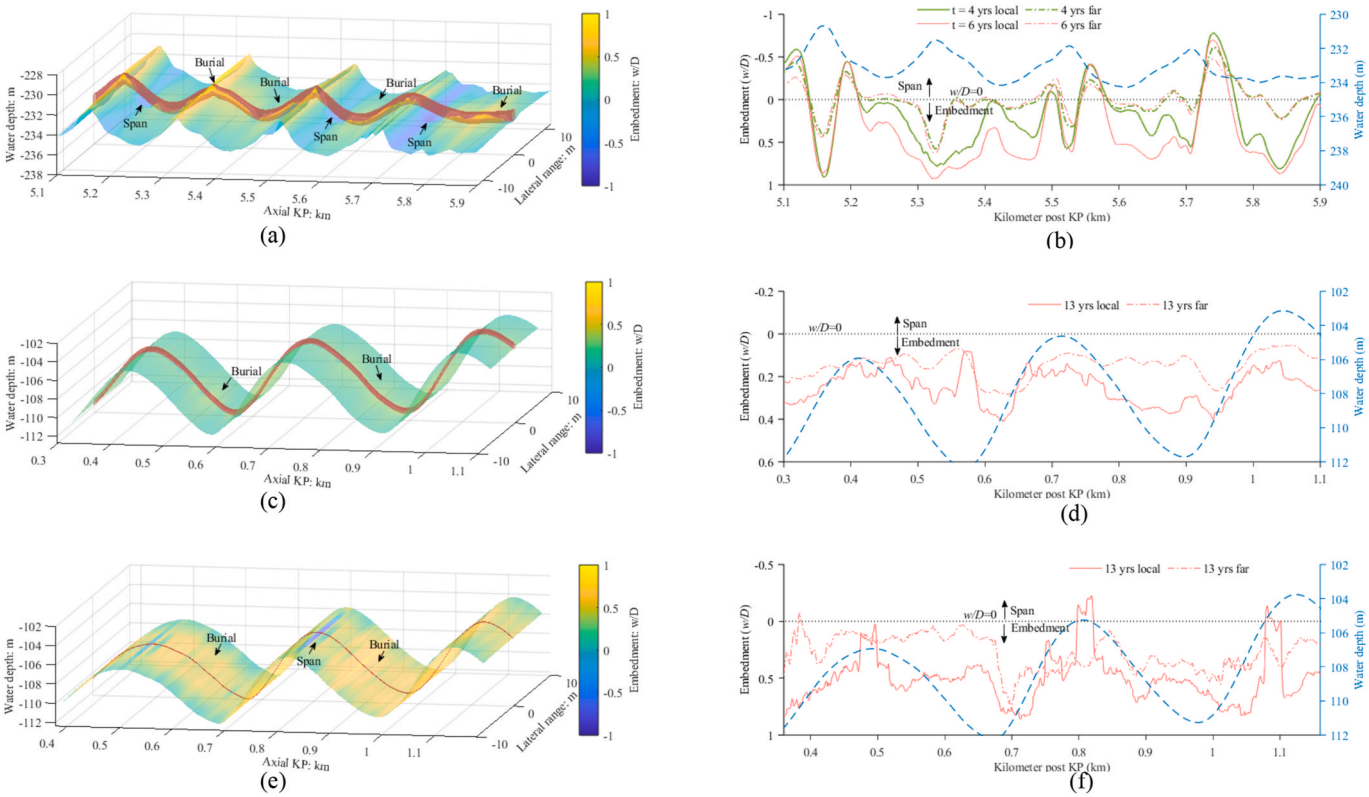

Fig. 6. Temporal changes of embedment (a) Pipeline A at t = 6 years (b) Pipeline A – embedment at t = 4 and 6 years (c) Pipeline B – 3D contour at t = 13 years (d) Pipeline B – embedment at t = 13 years (e) Pipeline C – 3D contour at t = 13 years (f) Pipeline C – embedment at t = 13 years.

that the pipeline was in continuous contact with the seabed. The broadly higher local *w/D* compared to the far *w/D* indicates partial burial from sediment mounding around the pipeline perimeter in the six years after lay, which is discussed later.

3.2. Time evolution of local and far embedment

The temporal changes of local and far embedment for each pipeline are introduced in Fig. 6 by showing the data over the same 800 m-long sections from the most recent and reliable point-listing data for each pipeline. For Pipeline A this survey was six years after installation and shows sagging into the sand wave troughs (Fig. 6a compared to Fig. 5a). This is influenced by the hydrotesting and operational weight increase of Pipeline A since the as-laid survey, as well as temporal effects. Significant burial from sediment accumulation alongside Pipeline A is also observed in both the sandwave peak and trough areas (similar to observations by Leckie et al. 2016), which leads to the increase of local *w/D* (Fig. 6b). Due to these two factors, the associated span lengths shorten significantly to ~30–50 m.

Fig. 6c and d shows that the embedment of Pipeline B also increases over the same period, particularly local to the pipe, which is also consistent with sediment being trapped around the pipeline.

Pipeline C also shows an increase in local embedment over the 7 years between the earliest and most recent survey (Fig. 6e). However, there is a reduction in embedment and a new ~24 m long span evident in the most recent survey at the sand wave peak at KP ~0.8, which can likely be attributed to local scour processes (i.e., removal of sediment around the pipeline by hydrodynamic forces).

3.3. Embedment evolution in the whole sand wave area

The observations highlighted in the selected 800 m sections of each pipeline that were presented in Figs. 5 and 6 have also been quantified for the whole sand wave area through statistical analysis of the full embedment dataset. Firstly, trends for the full length of each pipeline in the sand wave area are set out (Figs. 7 and 8), followed by examination of the pipeline burial conditions in the contact zones close to the sand wave peaks (Fig. 9).

Fig. 7 presents the frequency and cumulative distributions of both local and far embedment (*w/D*) of the three pipelines. The evolution with time of the embedment quantiles is shown in Fig. 8, which includes an additional data set at t = 4 years for Pipeline A. This data is discussed in the following sections.

3.3.1. Sand wave area 1

In Area 1, over 60 % of Pipeline A is in free span (i.e. local $w/D < 0$) in the as-laid condition, with ~10 % having a span depth above 1*D* (in this case ~1.2 m). Six years later, significant increase of local embedment and corresponding reduction of span length was observed, linked to both the increase in weight since laying (due to hydrotesting and operation) and sediment accumulation. The data shows that 2–3 % of the pipeline becomes fully buried (i.e., local $w/D \geq 1$), which occurs near the sand wave peaks, while the total span length halves, leaving only 30 % in span (Fig. 8a).

The change in pipe weight and axial load between pipelay (lighter, in tension) and operation (heavier, and with significant effective compression) is partly responsible for these changes, although the evident variations in pipeline span and embedment between 4 and 6 years after pipelay (see Fig. 8a) show that sediment mobility also plays a role.

3.3.2. Sand wave area 2

Pipelines B and C show a similar trend of increasing local embedment over time but have minimal spanning (<10 % of the length) throughout the survey period. The initial survey of Pipeline B shows higher far *w/D* compared to local *w/D* (by ~10 %) indicating a modest trench created during installation, or limited local scour in the 6 months between installation and the first survey (see Fig. 7b). By the 13-year survey, the median local *w/D* has increased by 0.2 but the median far w/D has decreased by 0.06. Other quantiles of local embedment also show a general increase with time, while the spanning ratio remained low and approximately constant (Fig. 8b).

For Pipeline C the median values of local and far embedment increase by 0.36 *D* and 0.1 *D*, respectively, between the 6th and 13th years (Fig. 7c), with other quantiles showing a similar trend (Fig. 8c). The slight increase in far embedment indicates potential pipeline lowering while the span proportion remained constant at ~10 %.

3.4. Embedment in peak and trough area of sand waves

To examine the contrasting behaviour at the peak and troughs of the sand waves, where the pipelines rest and span respectively, the embedment data was filtered to extract only the data over 10 % of the average sand wavelength, centred on the top of each peak and at the base of each trough (i.e., a length of ~17 m for Area 1 and Pipeline A, and ~28 m for Area 2 and Pipelines B and C). Fig. 9 indicates the change with time of the frequency and cumulative distribution of local embedment for each pipeline in the peak and trough regions.

Due to the aforementioned pipeline sagging and sediment burial process, the local embedment of Pipeline A increased over time in both the peaks and troughs (Fig. 9a). The median embedment ratio in the trough region evolved from −1 (i.e. spanning with a gap of 1 *D* below the pipeline) to 0.15 (i.e. embedded to 0.15 *D*). In the peak region, ~10 % of the pipeline was fully buried (local $w/D \geq 1$).

For the more flexible Pipelines B and C the peak region showed higher average embedment (by ~0.1 *D*) compared to the trough regions,

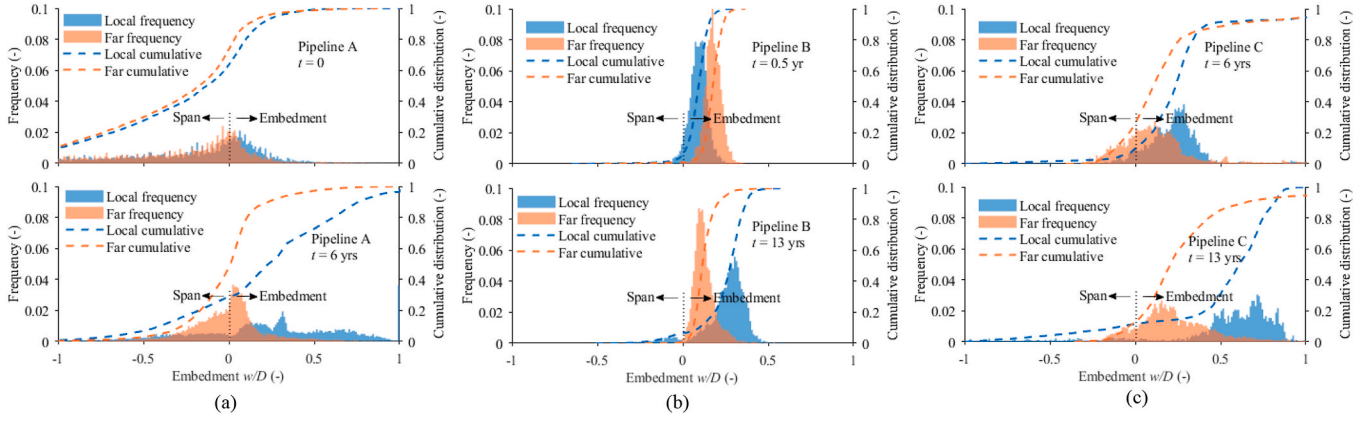

Fig. 7. Frequency and proportion curves for temporal changes of local and far embedments (a) Pipeline A (b) Pipeline B (c) Pipeline C.

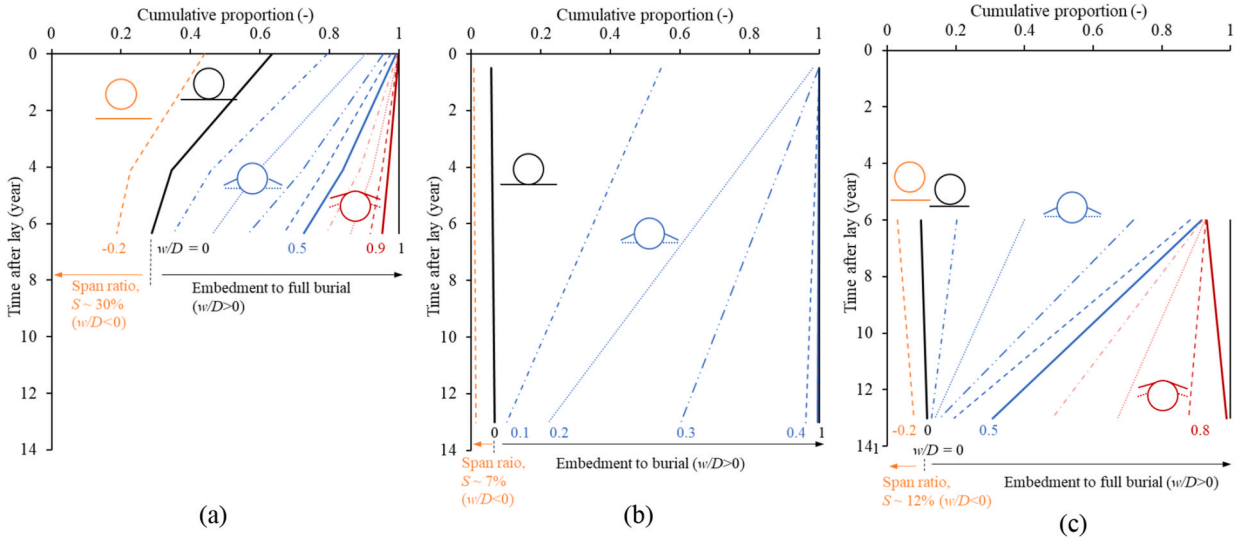

Fig. 8. Typical proportion plots of local embedment changes for (a) Pipeline A (b) Pipeline B (c) Pipeline C in sand wave areas.

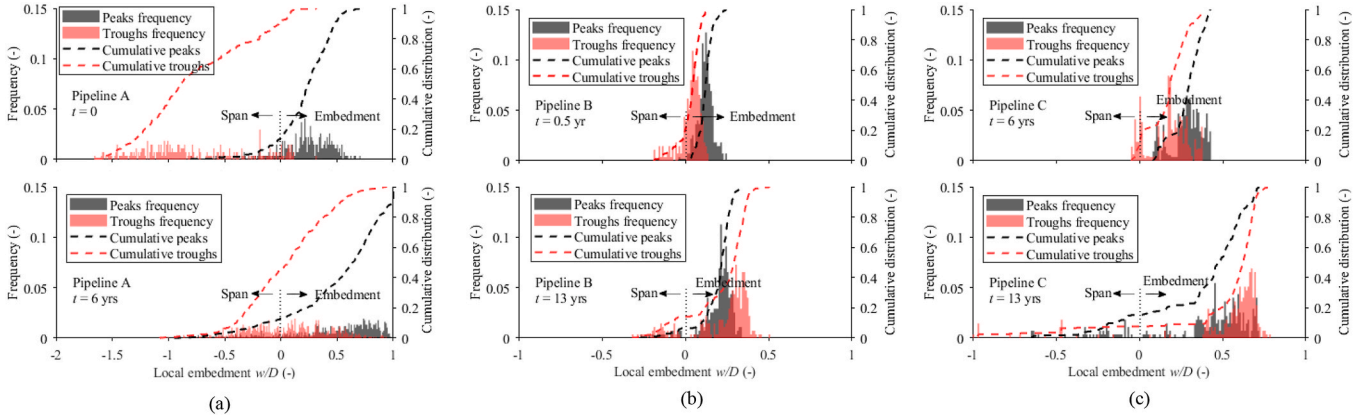

Fig. 9. Frequency and proportion curves of pipeline local embedments on peaks and troughs of sand wave area (a) Pipeline A (b) Pipeline B (c) Pipeline C.

both in the 0.5 year and 6 year surveys – and with both sets of embedment data increasing with time.

3.5. Summary

All three pipelines experienced temporal changes in embedment after installation. This is a response to different mechanisms, linked to (i) changes in pipe weight after laying, (ii) sediment mobility leading to scour (erosion) and deposition, and (iii) soil-structure interaction, with varying levels of sagging into the sand wave troughs linked to the different bending stiffness of the different pipelines and the increase in axial compression, particularly in Pipeline A, during operation. As a result, the more flexible Pipelines B and C conform more with the sand waves compared to Pipeline A.

Approximately 30 % of Pipeline A remained in span over the sand wave troughs. The most flexible pipeline (Pipeline C) is more than half buried, but with a few short areas of span that appear to result from local scouring events. Pipeline B shows intermediate trends of embedment and spanning. All three pipelines show a net increase in embedment, which in turn translates to increased seabed resistance and improved lateral stability. Although the survey times vary between pipelines, the observed trends of embedment changes are consistent with a broader database of pipelines in the same region.

The observed as-laid embedment and the subsequent temporal changes in embedment are further investigated in the following section, through comparisons with theory and design practice.

4. Interpretation and discussion

4.1. Selection of 'laydown' soil stiffness

4.1.1. Method of analysis

The as-laid embedment of pipelines and cables is predicted in design by (i) using a typical bearing failure equation (either a drained or undrained method e.g. DNV AS, 2021a) that links vertical seabed reaction force to embedment, and (ii) estimating the maximum vertical seabed reaction force during laying, V_{lay}, which is greater than the weight W'_{lay} due to the catenary configuration adopted. This enhancement factor is defined as $f_{lay} = V_{lay}/W'_{lay}$ and is calculated as follows (Randolph and White, 2008b):

$$f_{lay} = 0.6 + 0.4\left(\lambda^2 k/T_0\right)^{0.25} \quad \text{(Eq. 1)}$$

where T_0 is bottom lay tension, $\lambda = \sqrt{(EI/T_0)}$ is a characteristic length, and k is the linearised seabed stiffness, defined as the vertical seabed reaction force divided by embedment w:

$$k = V_{lay} \Big/ w = \left(f_{lay} W'_{lay}\right) \Big/ w \quad \text{(Eq. 2)}$$

For carbonate soil conditions (which are not covered by DNV AS, 2021a), the bearing capacity expression for drained conditions was

proposed in Zhang et al. (2002) to take the form of a bearing modulus K_{vp} defined as:

$$K_{vp} = V_{lay}/(D \cdot w) \quad \text{(Eq. 3)}$$

where the value of K_{vp} depends on the properties of the surficial sediment (Bransby et al., 2020).

While equations (1)–(3) provide the necessary elements to define embedment from a static lay perspective, the dynamic aspects of the laying process may further increase embedment. For drained soil conditions, this occurs through the scraping of soil aside as the pipeline oscillates close to the touchdown point during laying (e.g. Westgate et al., 2012). In comparison, the mechanism changes to soil softening predominantly for undrained conditions, and both mechanisms need consideration for intermediate drainage conditions. The approach adopted in the present study is to incorporate any dynamic lay effects into a back-analysed equivalent bearing modulus, K_{vd} (based on Equation (3) but using the embedment w after pipe-lay). Equations (1)–(3) have been used to calculate K_{vd} from the observed distributions of as-laid embedment values with results presented in the following sections.

4.1.2. Back-calculated bearing modulus values, K_{vd}

Fig. 10 introduces the interpreted K_{vd} values for the seabed along Pipeline B in both sand wave area 2 and an adjacent area of flat seabed (with similar soil conditions to allow direct comparison and the soil is assumed to be drained during lay). Results are shown based on both the far embedment (as the benchmark value) and the local embedment (to quantify potential trench or heave effect locally during pipelaying). The wider range of K_{vd} based on local embedment indicates the uncertainty to be considered in pipelaying. The median (P50) value of K_{vd} in the flat seabed region and the sand wave field are similar at around 55 kPa/m. The P5 to P95 range (i.e., 95 %–5 % exceedance value) of K_{vd} in the sand wave field and flat seabed show broadly comparable results between 35 and 100 kPa/m.

The back-calculated median K_{vd} value is around 7 times smaller than the stated bearing modulus of 350 kPa/m reported by Zhang et al. (2001) for carbonate sand, based on penetration resistances measured

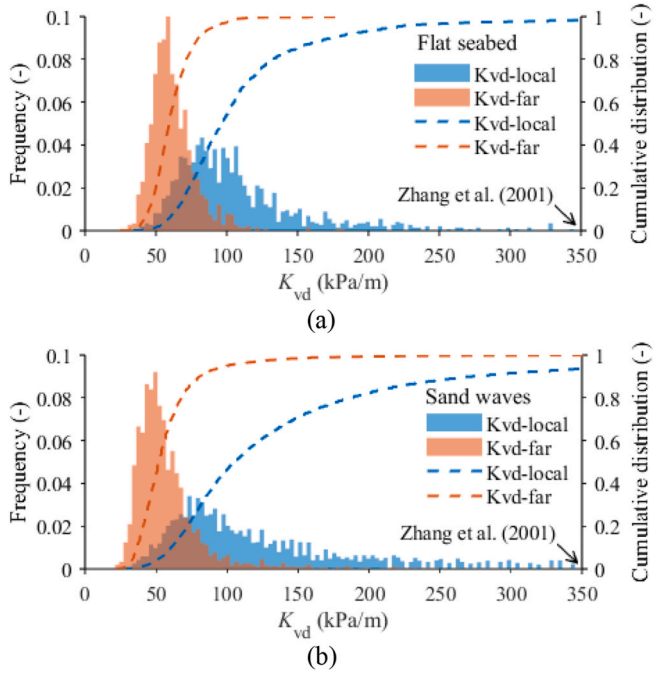

Fig. 10. Back-calculated soil bearing modulus values for pipeline B in (a) flat seabed section (b) sand waves.

during monotonic 'static' plastic penetration of a pipe segment in a geotechnical centrifuge. However this recommendation was given for one particular carbonate sand sample and the bearing modulus is expected to vary for different soil types and states (e.g. Bransby et al., 2020). Also, following the design practice for drained as-laid embedment (DNV AS, 2021a), with the inputs in Tables 1 and 2, would yield a design value of stiffness more than 10 times higher than that estimated from the observed data (see also Hou et al., 2023a).

4.1.3. Correlation between bearing modulus values and cone gradient

Fig. 11 presents a correlation between best fit cone gradient values K_{qc} (in kPa/m) in the top 0.5 m of the seabed (see Fig. 4 for the raw data and an example fit) and the back-calculated equivalent dynamic bearing modulus K_{vd} for Pipeline B – based on far embedment for the 50-m-long pipeline section closest to each CPT location. The data extends to the flat seabed zones beyond the sand wave fields.

A broadly linear correlation between K_{vd} and K_{qc} is observed, matching similar trends for the vertical stiffness of foundations on carbonate sediments (Finnie and Randolph, 1994; Zhang et al., 2001) and pipelines in silica sand (Bransby et al., 2021). Further investigation into the use of CPT data to predict pipeline embedment in carbonate soils is reported by Taner et al. (2024) using a larger database.

4.2. Bending moment and seabed reaction

4.2.1. Method of analysis

The pipe crown elevation data allows the distribution of both bending moment (M) and the seabed reaction force (q_{soil}) to be determined along the pipeline. The bending moment (M) is calculated from the second differential of crown depth (i.e., the curvature of the pipeline):

$$M = EI \cdot \kappa = EI \cdot z_w'' = EI \cdot \frac{\delta^2 z_w}{\delta x^2} \quad \text{(Eq. 4)}$$

where EI is the flexural rigidity of the pipeline, κ is the bending curvature, z_w is the water depth of the pipeline top and x is the position along the pipeline axis. This approach is valid as the bending loads remain well within the limit of proportionality.

The seabed reaction force distribution ($q_{soil}(x)$, in kN/m) can be obtained by further differentiation of the pipeline profile assuming that the pipeline behaves as an elastic beam:

$$q_{soil} = -EI \cdot \frac{\delta^4 z_w}{\delta x^4} + T_a \cdot \frac{\delta^2 z_w}{\delta x^2} + W' \quad \text{(Eq. 5)}$$

where T_a is the axial force in the pipeline (which may change from positive tension after lay to negative compression in operation), and W' is the pipeline submerged weight.

The measured crown depth data is influenced by survey noise,

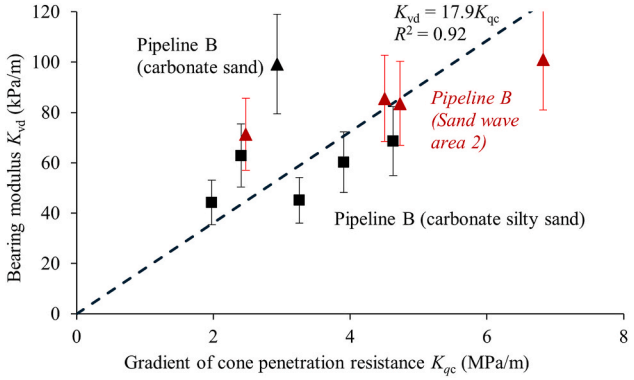

Fig. 11. Correlation between cone gradient values (K_{qc}) and back-calculated dynamic soil bearing modulus (K_{vd}).

whereas the true configuration of the pipeline is smooth and continuous. These survey errors were screened out using a Savitzky-Golay filter (Schafer, 2011), with a window size of 80 m (approximately half the mean wavelength of the sand waves).

4.2.2. Pipeline on flat seabed

Using this methodology, the evolution of pipeline moment and seabed resistance of a 1 km-long section of Pipeline A on a flat seabed outside the sand wave area (but with similar geotechnical and metocean conditions) is shown on Fig. 12.

The deduced bending moment fluctuates around an average of zero, with a larger range in the 4th and 6th year. The corresponding distribution of deduced vertical seabed reaction shows broadly steady values that are consistent with the associated submerged weight, confirming the reasonableness of this structural analysis approach. By comparing the seabed reaction for the cases with zero tension with either the lay tension (T_o) or an operational compression of 2 MN applied, the interpreted seabed response is shown to be relatively insensitive to axial force for the flat seabed. The maximum moment is ~1 MN m which represents only 10 % of the moment limit of the pipeline (DNV AS, 2021d).

4.2.3. Pipeline traversing a sand wave section

The same methodology is used to investigate bending moment and seabed reaction force changes for a 1-km section of Pipeline A in sand wave area 1 from the as-laid condition to 6 years after lay (Fig. 13).

4.2.4. Distribution of bending moments and seabed reaction

In the as-laid condition (Fig. 13a), there is significant hogging bending moment over the sand wave peaks, with sagging between the peaks. The deduced seabed reaction forces show small non-zero values when in span, which reflects errors from the quadruple differentiation of the smoothed displacement profile. However, the reaction forces on the sand wave peaks are significantly larger than the pipeline self-weight, as expected. There is a small influence (up to 20 %) in the seabed reactions based on the assumed axial force, and of either zero or full lay tension.

By the 4-year and 6-year surveys (Fig. 13b and c) the bending moment and seabed reactions increase significantly in the sand wave peak region. The increased pipeline self-weight (from empty as-laid, to flooded and operational weights) and change in axial force (between the lay condition and the operational 4-year survey) cause the pipeline to sag and conform better with the sand wave geometry, reducing the free-span lengths.

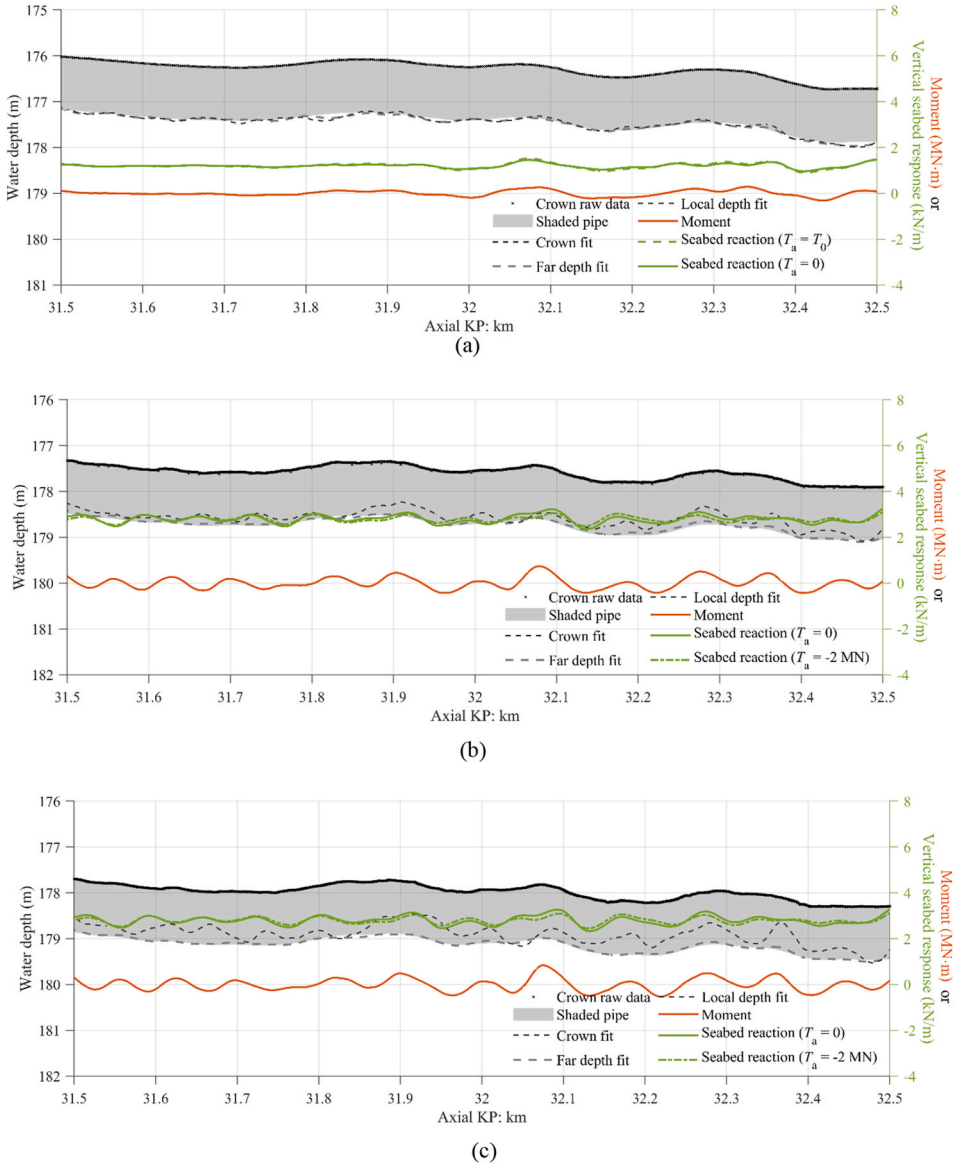

Fig. 12. Pipeline geometry, embedment conditions and bending moment on a flat seabed region (a) as-laid (b) after 4 years (c) after 6 years.

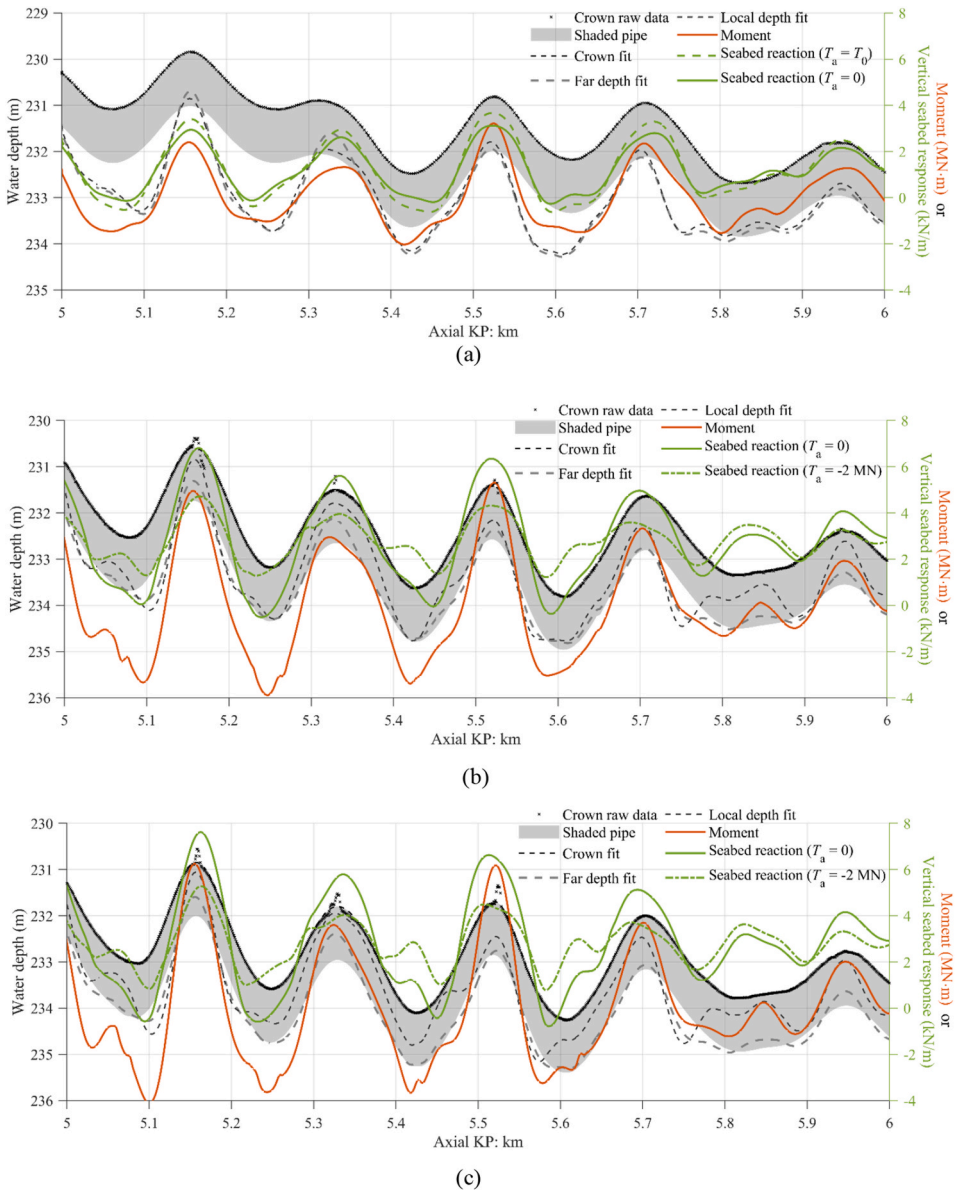

Fig. 13. Pipeline geometry, embedment conditions and bending moment on a sand wave area (a) as-laid (b) after 4 years (c) after 6 years.

Fig. 14a shows that the maximum and minimum bending moment on each of the five sand wave peaks and troughs in the 1-km section increases by 2–2.5 times from the as-laid condition to the 4th year survey, then stabilises. The difference in moment between adjacent hogging and sagging points correlates well with the associated pipeline elevation differences over the sand wave, regardless of the time (Fig. 14b).

The distribution of bending moment across the whole of sand wave area 1 is summarised in Fig. 15 for the as-laid condition and after six years. As shown, there is a wider range of bending moment after six years due to the pipeline sagging into the sand wave troughs.

The mean strain level resulting from the P95 curvature remains within the safe design region of less than ~±0.2 % typically adopted for concrete coating failure (DNV AS, 2021d) with a safety factor of ~4. This indicates the curvatures and resulting moment remain safe after pipeline installation.

4.3. Evolution of free spans

Changes in the number (N_{span}) and length (L_{span}) of the free spans for Pipeline A in sand wave area 1 are further summarised in Fig. 16. The maximum L_{span} halves from 160 m in the as-laid condition to ~80 m in the 6th year, with a corresponding reduction in the P50 value from ~62 m (at $t = 0$) to ~35 m (at $t = 4$ years) and then ~30 m (at $t = 6$ years). Meanwhile, N_{span} only reduces slightly, by around 14 % over 6 years.

The reduction in L_{span} is due to pipeline sagging caused by the increased weight and effective axial compression in operation, as well as sinking of the pipe into the sand wave crests and deposition of sand around the pipeline. In a few cases a long span touches down at the midspan point, splitting into two shorter spans. In more cases, the entire span touches down and sediment mobility leads to deposition around the pipeline, with the span subsequently eliminated.

Tidal currents may introduce vortex-induced-vibrations on long spans, which leads to potential fatigue damage accumulation. The reduced length and number of spans can either (i) reduce the possible occurrence of vortex-induced-vibrations, or (ii) change the hotspot of the fatigue accumulation zone. These effects reduce the requirement for intervention work and may also improve hydrodynamic stability as investigated below.

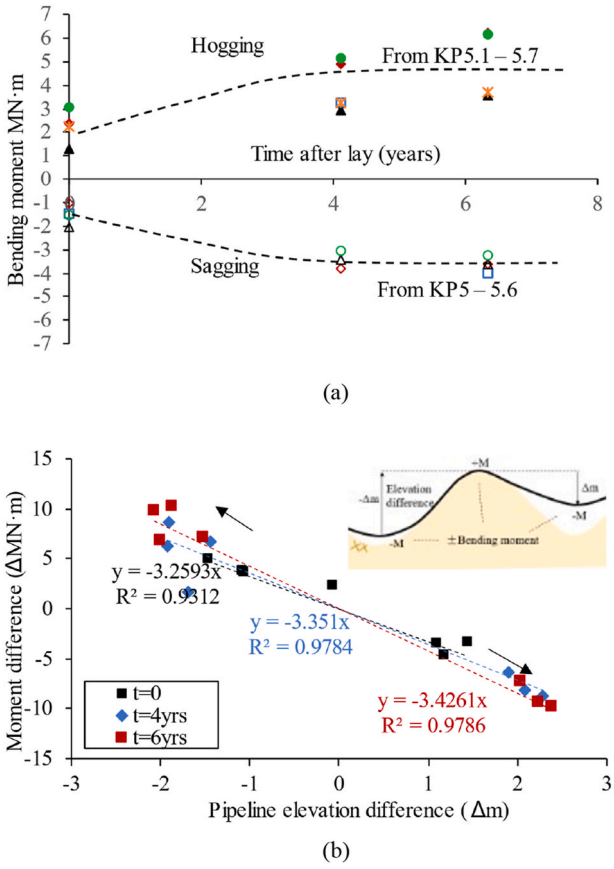

Fig. 14. (a) Distribution of bending moment in sand wave region (b) Correlation of moment difference and sand wave elevation difference.

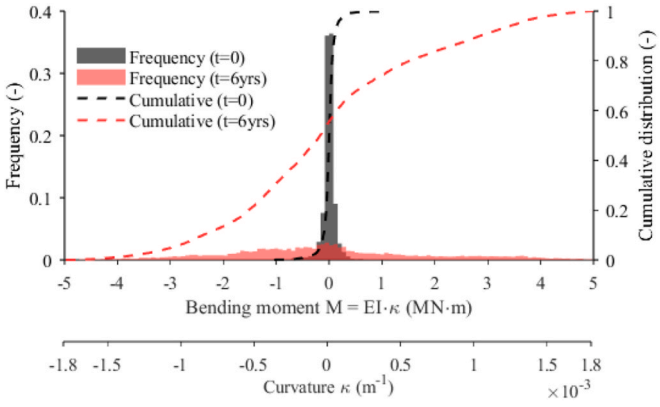

Fig. 15. Evolution of frequency and cumulative distribution of bending moment (M = EI·κ) for pipeline A.

4.4. Stability of pipelines under hydrodynamic forces

4.4.1. Method of analysis

To quantify the influence of the changing span ratio S (i.e. proportion of pipeline section in span over the total pipeline length) and embedment w/D (defined in Fig. 8) on the hydrodynamic stability of the pipeline, equilibrium models for vertical and lateral stability are used. Firstly, the average lift force ($\overline{F_L}$) is compared to the unit weight of the pipeline ($W'_{as-laid}$ or $W'_{operational}$) as a length-averaged check of vertical equilibrium. Secondly, the length-averaged lateral equilibrium is checked by comparing the averaged drag force ($\overline{F_D}$) to the available lateral soil resistance ($\overline{F_S}$). These length-averaged analyses cannot be

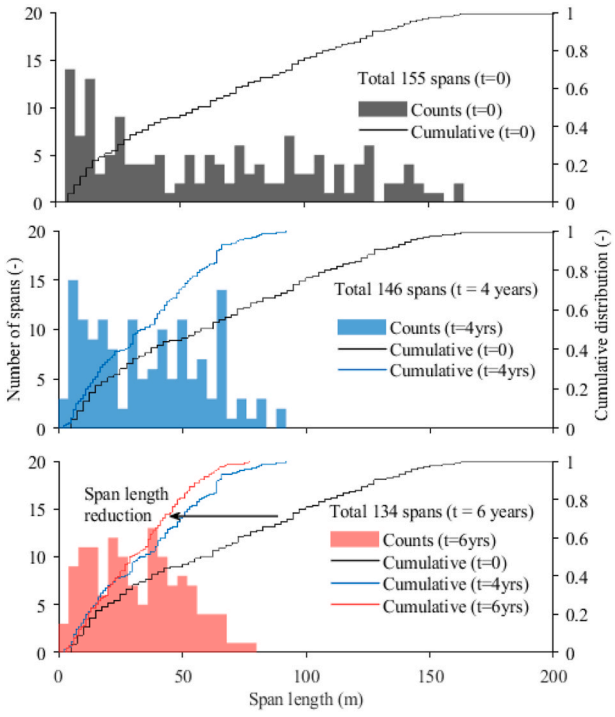

Fig. 16. Evolution of span length for pipeline A in sand wave area 1.

used to assure the local stability of a particular length of pipeline without calibration to establish an allowable utilisation, as for the generalised method of stability analysis (DNV AS, 2021b; 2021c). However, they do allow temporal trends in stability to be determined (Leckie et al., 2018).

The lift and drag force components are calculated as:

$$F_L = 0.5\varphi_L \rho_w C_L D U_c^2 \quad \text{(Eq. 6)}$$

$$F_D = 0.5\varphi_D \rho_w C_D D U_c^2 \quad \text{(Eq. 7)}$$

$$\varphi_L = \begin{cases} 1 & \text{if } w/D < 0.1 \text{ and all } e/D \\ 1 - 1.3\cdot\left(\dfrac{w}{D} - 0.1\right) & \text{if } 0.1 \le w/D \le 0.869 \\ 0 & \text{if } w/D > 0.869 \end{cases} \quad \text{(Eq. 8)}$$

$$\varphi_D = \begin{cases} 1 & \text{if } 0.8 \le e/D \\ 0.9 + \dfrac{0.5}{1 + 5\cdot e/D} & \text{if } 0 < e/D < 0.8 \\ max\,(1 - 1.4\cdot w/D, 0.3) & \text{if } 0 \le w/D \le 1 \end{cases} \quad \text{(Eq. 9)}$$

where ρ_w is the sea water density, C_L and C_D are lift and drag coefficients and were taken as 0.5 and 1.5, φ_L and φ_D are force reduction factors that vary with pipeline embedment (w) or span height (e) following DNV-AS (2021b, c) as below.

U_c is the current speed considering the boundary layer effect and is derived as below:

$$U_C(z) = \frac{u_*}{0.4} \ln\left(\frac{z}{z_0}\right) \quad \text{(Eq. 10)}$$

where $U_c(z)$ is the current velocity at the height z above the seabed (see Fig. 1a), u_* is the friction velocity and z_0 is the seabed roughness length. z_0 is adopted as 0.4 mm (Soulsby and Whitehouse, 1997) and u_* is fitted for each pipeline to match the input current speed at 1 m above the seabed.

The lateral soil resistance, F_S, is assumed to be drained and approximated by the following equation:

$$F_S = \mu(W' - F_L) + 0.5K_P\gamma' w^2 \quad \text{(Eq. 11)}$$

where μ is the interface friction coefficient and assumed to be 0.8, and K_p is an empirical coefficient considering passive soil resistance and is assumed as 5.8 (representing the value using the Rankine equation ($K_p = \tan^2(45 + \Phi'/2)$) for a friction angle of 45° which is typical for carbonate sediments).

4.4.2. Calculated hydrodynamic stability

Fig. 17a to c shows load paths (as dashed lines) of equivalent length-averaged drag force ($\overline{F_D}$) versus vertical force ($W' - \overline{F_L}$) for a range of different perpendicular current speeds (at 1 m above seabed) based on Equations (6)–(11), accounting for the embedment and spanning of the three pipelines at the time of their first and last surveys (see Fig. 8). Also shown is the available soil resistance envelope at the same time (as solid lines) – which allows the critical steady current to destabilise each pipeline at the time of each survey to be estimated. For example, Pipeline A in the as-laid condition would require a velocity, U_{stab} = 1.1 m/s (Fig. 17a), whereas a velocity of 3.7 m/s (1 m above seabed) is required to destabilise the pipeline six years later. This increase is due to higher embedment and reduced span length in the operational state, as well as the increase in pipeline self-weight. There are less dramatic, but still significant, increases in stability for pipelines B and C with time, with U_{stab} increasing.

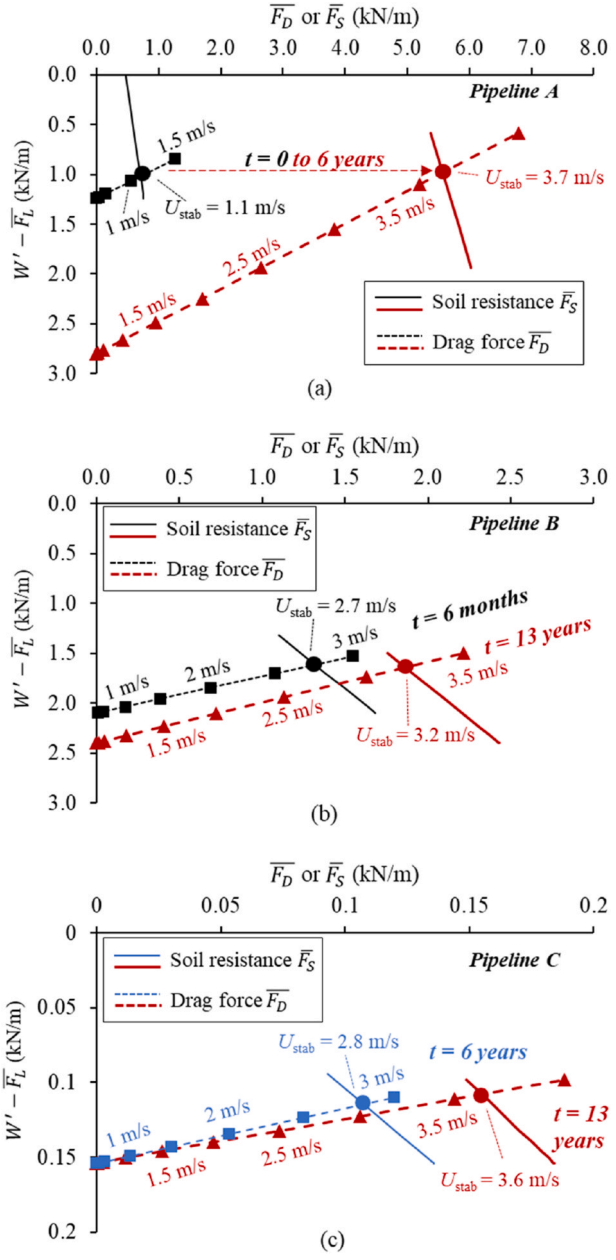

Fig. 17. Temporal changes of loading path (drag force $\overline{F_D}$) and failure limit (soil resistance $\overline{F_S}$) versus vertical contact weight ($W' - \overline{F_L}$) for (a) pipeline A (b) pipeline B and (c) pipeline C.

4.4.3. Summary

The calculation method adopted here does not fully reflect real pipeline behaviour, because (i) by using a length-averaged approach it is assumed that the spans can transmit the loading to the grounded pipeline, and (ii) the stability factors are based on an assumption that the pipeline embedment remains unchanged during any storm or flow velocity build-up. However, these qualifying assumptions do not invalidate the observed stability trends in different conditions and so this approach, that allows quick assessment of the pipelines for a range of time intervals, is used.

The pipelines become increasingly stable due to temporal changes in embedment. If the pipeline embedment remains unchanged during any storm or flow velocity build-up, the design approach could allow the temporary less-stable as-laid condition to be compensated by the significant stability benefits from increases in embedment soon after lay (e.g. within the typical period before operation begins, which is around 6 months, and very brief compared to the design life of the pipeline or cable). This approach could reduce the requirements for primary or secondary stabilisation of a pipeline or cable.

The prediction accuracy of these changes may be low in the front-end engineering design stage, but can be improved with detailed metocean, geotechnical and sediment mobility analysis, and can be supported by systematic back-analysis of field data of the form shown in this paper.

4.5. Stability of seabed and onset of scour

4.5.1. Method of analysis

An onset criterion is often used to evaluate the potential for local scour processes to occur, as given by (Sumer and Fredsøe, 2002):

$$\frac{U_{cr}^2}{gD(1-n)(s-1)} = 0.025 \exp\left[9\left(\frac{w}{D}\right)^{0.5}\right] \quad \text{(Eq. 12)}$$

where U_{cr} is the critical undisturbed flow velocity at the level of the top of the pipeline for the onset of scour, g is gravitational acceleration, D is the external pipeline diameter, n is the soil porosity, s is the specific gravity of the soil, and w is the pipeline local embedment. This relationship may not be directly applicable to the carbonate sediments that show different erosion resistance, particularly when there are significant fines content (e.g. Mohr et al., 2016; Watson et al., 2019), but is used here as an approximation of the behaviour and to demonstrate the assessment approach.

To link the measured current speed at each site, field soil conditions (given in Tables 1 and 2) and observed pipeline embedment, the components of Equation (12) are evaluated and compared with the onset criterion. The steady current speed at the top of each pipeline is scaled from the measured current speed at 1 m above seabed in each site (using a 0.01 % exceedance value denoted as U_{max} in Table 2). The resulting embedment, w, below which there will be the onset of scour, are compared with the P15 or P50 embedment values (from Fig. 9) for the sand wave peaks and troughs, respectively, to identify the flow conditions at which scour may begin.

4.5.2. Capability to prevent scour onset

Fig. 18a shows that all three pipelines evolve away from the unstable zone of scour occurrence as the P50 embedment values in the sand wave peaks increases. The majority of each pipeline length is in a condition of

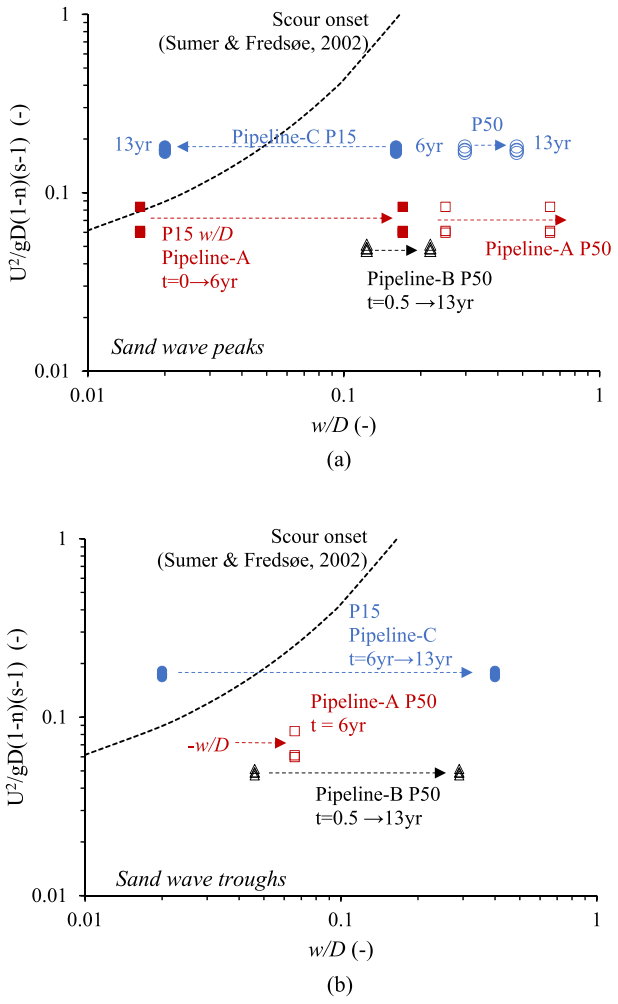

Fig. 18. Back-calculated onset of scour for surface-laid pipelines versus (a) peak embedment (b) trough embedment of sand waves.

no scour onset. Around 15 % of Pipeline A (representative of the P15 embedment value) is within the scour onset zone in the as-laid condition when subject to the 0.01 % exceedance velocity, but the sediment burial process dominates in the post-installation stage and moves the pipeline into a less scourable condition. In contrast, the P15 embedment of Pipeline C reduces with time and raises the proportion of the pipeline in a scourable condition.

For the sand wave troughs of Pipeline A in Fig. 18b, the free span gives a negative P50 value for the as-laid condition (thus not shown here due to the log scale), and the increased pipeline P50 embedment generally leads to stable conditions by the 6th year. The greater increase of trough embedment of Pipeline B leads to a less scourable condition versus that in the peak regions. The P15 embedment of Pipeline C in the sand wave troughs moves out of the unstable condition from the 6th year, which gives an opposite trend to that in the sand wave peaks. This indicates that the sand wave trough region may provide more shielding effects to prevent scour onset, which are important for smaller diameter pipelines and power cables with similar diameter ranges (Cheng et al., 2016).

In both sand wave peaks and troughs, the current velocity leading to scour onset is significantly less than will cause drag force-induced pipeline instability (see Fig. 17). For example, the least hydrodynamically stable pipeline (Pipeline A at $t = 0$) requires a velocity U_{stab} of 1.1 m/s to cause gross movement compared to a 0.01 % non-exceedance velocity on site of U_{max} of 0.71 m/s (both velocities at 1 m above seabed). This indicates that instability of the seabed (through scour onset) is a more probable than instability of the pipeline (under hydrodynamic lift and drag force) in this case study, which aligns with results reported by Palmer (1996), and Griffiths et al. (2018).

5. Conclusions

This paper provides systematic interpretation of field embedment data for three different pipelines (with nominal diameters of 4 inches, 20 inches and 42 inches) installed in two different sand wave areas and tracks temporal changes in embedment from installation to a maximum duration of 13 years later. The associated embedment, seabed reaction forces and pipeline structural responses are interpreted from this collection of field survey data, leading to the following conclusions:

- In order to 'predict' as-laid embedment values, lay-down soil stiffness values need to be more than 10 times less stiff than the recommended values for a drained soil response (e.g. DNV AS, 2021a). This is linked to the dynamic lay process, the effects of which are not directly captured in code-recommended design approaches for drained soil conditions. In addition, the back-calculated soil bearing modulus shows a linear correlation with gradient of cone tip resistance – which indicates the potential for estimation of drained as-laid embedment through site-specific soil data rather than based on generic empirical factors.
- All three pipelines experience changes in embedment and spanning from the as-laid condition, due to the changing pipe weight during pre-commissioning and operation, and also due to sediment mobility and soil-structure interaction. The associated increase of pipeline curvature and axial strains over the sand waves area remained well below design limits for these pipelines.
- The pipeline sagging, sediment deposition and soil-structure interaction process around the most rigid pipeline led to (i) a two-fold reduction of length of free-spans and (ii) a ~15 % reduction of the number of spans compared to the as-laid condition. Consequently, fewer free-span interventions and therefore less expenditure may be required if the fatigue life of the initial spans can be shown to exceed the time required for these spans to shorten sufficiently to prevent any further fatigue accumulation.
- An efficient method is developed to track pipeline bending moments and seabed reactions based on the pipeline crown depth information provided in standard inspection surveys. The method is well-suited to free-spanning pipelines on sand waves.
- Using length-averaged approaches to assess hydrodynamic stability, it is shown that the changes to pipeline embedment and spanning in the sand wave areas lead to an increase in hydrodynamic stability by up to 10 times. Furthermore, these changes protect the pipeline from the onset of scour.

The general field-observation analysis approach used in the paper adds to the understanding of pipeline stability in sand wave areas, supporting the development of prediction methods that unlock more efficient design and maintenance strategies by allowing for seabed mobility effects.

CRediT authorship contribution statement

Zhechen Hou: Writing – original draft, Visualization, Formal analysis, Data curation, Conceptualization. **Fraser Bransby:** Writing – review & editing, Supervision, Methodology, Conceptualization. **David White:** Writing – review & editing, Methodology, Conceptualization. **Phillip Watson:** Writing – review & editing, Supervision, Resources, Funding acquisition. **Andrew Rathbone:** Writing – review & editing, Validation. **Han Eng Low:** Writing – review & editing, Validation.

Declaration of competing interest

The authors declare that they have no known competing financial interests or personal relationships that could have appeared to influence the work reported in this paper.

Acknowledgements

This research is supported by the ARC ITRH for Transforming energy Infrastructure through Digital Engineering (TIDE, http://TIDE.edu.au) which is led by The University of Western Australia, delivered with The University of Wollongong and several other Australian and International research partners, and funded by the Australian Research Council, INPEX Operations Australia, Shell Australia, Woodside Energy, Fugro Australia Marine, Wood Australia, RPS Group, Bureau Veritas and Lloyd's Register Global Technology (Grant No. IH200100009).

The second author holds the Fugro Chair, whose support is gratefully acknowledged. The third author acknowledges the support of the EPSRC Offshore Renewable Energy Supergen Hub (EPSRC Grant No. EP/Y016297/1). The fourth author leads the Shell Chair in Offshore Engineering research team at The University of Western Australia, which is sponsored by Shell Australia.

References

Adnyani, L.P., Draper, S., An, H., Cheng, L., 2023. Simulating model-scale bedforms and their interaction with subsea pipelines and cables. In: 11th International Conference on Scour and Erosion (ICSE-11).

Allen, J.R.L., 1980. Sand waves: a model of origin and internal structure. Sediment. Geol. 26 (4), 281–328. https://doi.org/10.1016/0037-0738(80)90022-6.

An, H.W., Luo, C.C., Cheng, L., White, D.J., 2013. A new facility for studying ocean-structure–seabed interactions: the O-tube. Coast. Eng. 82, 88–101. https://doi.org/10.1016/J.COASTALENG.2013.08.008.

Ardelean, M., Minnebo, P., 2015. HVDC Submarine Power Cables in the World. Joint Research Center.

Australian Government, 2025. Digital Atlas of Australia. https://digital.atlas.gov.au/.

Bransby, M.F., Brown, M.J., Hatherley, A., Lauder, K., 2010. Pipeline plough performance in sand waves. Part 1: model testing. Can. Geotech. J. 47 (1), 49–64. https://doi.org/10.1139/T09-077.

Bransby, M.F., Rodriguez, A.B., Zhou, H.J., Tom, J.G., Low, H.E., White, D.J., 2014. Sediment mobility effects on seabed resistance for unburied pipelines. In: Proc. Offshore Technol. Conf.. https://doi.org/10.4043/25287-ms. *Paper OTC 25287*.

Bransby, M.F., Low, H.E., Zhu, F.Y., Clavaud, R., White, D.J., 2020. Pipe-soil interaction for surface-laid pipelines in carbonate sediments. Proc. 4th Int. Symp. on Frontiers in Offshore Geotechnics, pp. 1690–1704.

Bransby, M.F., Low, H.E., O'Loughlin, C.D., Bhatti, F., Aljabury, N., 2021. Using near-surface CPT data to predict pipeline embedment in sands. In: 20th Int. Conf. on Soil Mechanics and Geotechnical Engineering., pp. 2607–2613. Sydney, Australia.

Bruschi, R., Drago, M., Venturi, M., Jiao, G., Sotberg, T., 1997. Pipeline reliability across erodible/active seabeds. In: Proceedings of the Annual Offshore Technology Conference, vol. 4. https://doi.org/10.4043/8493-MS.

Cheng, L., Yeow, K., Zhang, Z.P., Teng, B., 2009. Three-dimensional scour below offshore pipelines in steady currents. Coast. Eng. 56 (5–6), 577–590. https://doi.org/10.1016/J.COASTALENG.2008.12.004.

Cheng, L., An, H.W., Draper, S., White, D., 2016. Effect of wave boundary layer on hydrodynamic forces on small diameter pipelines. Ocean Eng. 125, 26–30. https://doi.org/10.1016/J.OCEANENG.2016.07.016.

Cheuk, C.Y., White, D.J., 2011. Modelling the dynamic embedment of seabed pipelines. Geotechnique 61 (1), 39–57. https://doi.org/10.1680/geot.8.P.148.

Dix, J.K., Hughes, T.J., Emeana, C.J., Pilgrim, J.A., Henstock, T.J., Gernon, T.M., Thompson, C.E.L., Vardy, M.E., 2017. Substrate controls on the life-time performance of marine HV cables. In: Offshore Site Investigation Geotechnics 8th International Conference Proceedings, pp. 88–107. https://doi.org/10.3723/OSIG17.088.

DNV, A.S., 2021a. Pipe-soil interaction for submarine pipelines. DNV-RP-F114.

DNV, A.S., 2021b. On-bottom Stability Design of Submarine Pipelines, Cables and Umbilicals. DNV-RP-F109.

DNV AS, 2021c. Free Spanning Pipelines. DNV-RP-F105.

DNV, A.S., 2021d. Submarine Pipeline Systems. DNV-ST-F101.

DNV AS, 2021e. Global Buckling of Submarine Pipelines. DNV-RP-F110.

Finnie, I.M.S., Randolph, M.F., 1994. Punch-through and liquefaction induced failure of shallow foundations on calcareous sediments. In: Proc. Int. Conf. on Behavior of Offshore Structures. BOSS'94, Boston, pp. 217–230.

Flemming, B.W., 1988. Zur Klassifikation subaquatischer, strömungstransversaler Transportkörper. In: Conference: Sediment 88 Volume: Bochumer Geologische Und Geotechnische Arbeiten, vol. 29, pp. 44–47, 29.

Griffiths, T., Draper, S., White, D.J., Cheng, L., An, H.W., Fogliani, A., 2018. Improved stability design of subsea pipelines on Mobile seabeds: learnings from the STABLEpipe JIP. In: Proceedings of the International Conference on Offshore Mechanics and Arctic Engineering - OMAE, vol. 5. https://doi.org/10.1115/OMAE2018-77217.

Hou, Z., Bransby, M.F., Watson, P.G., White, D.J., Ballard, J.C., Delvosal, P., Denis, R., Low, H.E., 2023a. Predicting the As-Laid embedment of surface-laid pipelines and cables in sand wave regions. In: ASME 2023 42nd International Conference on Ocean, Offshore and Arctic Engineering. https://doi.org/10.1115/OMAE2023-104434.

Hou, Z., Bransby, M.F., Watson, P.G., White, D.J., Low, H.E., Rathbone, A., 2023b. Operational integrity of pipelines on mobile seabeds: using survey data to explore trends of changing pipeline embedment and span evolution. In: In Proc. of the 9th Int. Offshore Site Investigation and Geotech. Conf.: Innovative Geotechnologies for Energy Transition, pp. 563–570. https://doi.org/10.3723/VPFW4060.

Huang, J., Zou, X., Li, L.W., Ragnar, T.I., Liu, Z.H., Romke, B., 2020. Subsea pipeline engineering challenges in sand wave area: the lufeng feed project. Proceedings of the International Conference on Offshore Mechanics and Arctic Engineering - OMAE 4. https://doi.org/10.1115/OMAE2020-18960.

Lebrec, U., Riera, R., Paumard, V., O'leary, M.J., Lang, S.C., 2022. Automatic mapping and characterisation of linear depositional bedforms: theory and application using bathymetry from the North west shelf of Australia. Remote Sens. 14 (2), 280. https://doi.org/10.3390/RS14020280/S1.

Leckie, S.H.F., Draper, S., White, D.J., Cheng, L., Fogliani, A., 2015. Lifelong embedment and spanning of a pipeline on a mobile seabed. Coast. Eng. 95, 130–146. https://doi.org/10.1016/J.COASTALENG.2014.10.003.

Leckie, S.H.F., Mohr, H., Draper, S., McLean, D.L., White, D.J., Cheng, L., 2016a. Sedimentation-induced burial of subsea pipelines: observations from field data and laboratory experiments. Coast. Eng. 114, 137–158. https://doi.org/10.1016/J.COASTALENG.2016.04.017.

Leckie, S.H.F., White, D.J., Draper, S., Cheng, L., 2016b. Unlocking the benefits of long-term pipeline-embedment processes: image analysis–based processing of historic survey data. J. Pipeline Syst. Eng. Pract. 7 (4), 04016008. https://doi.org/10.1061/(ASCE)PS.1949-1204.0000242.

Leckie, S.H.F., Draper, S., White, D.J., Cheng, L., Griffiths, T., Fogliani, A., 2018. Observed changes to the stability of a subsea pipeline caused by seabed mobility. Ocean Eng. 169, 159–176. https://doi.org/10.1016/J.OCEANENG.2018.07.059.

Low, H.E., Anderson, B., Bransby, F., 2018. Pipe-soil interaction at engineered lateral buckle touchdown zones. Offshore Technology Conference Asia 2018, OTCA 2018, pp. 20–23. https://doi.org/10.4043/28511-MS.

Madeley, C., Lombardo, D., Czajko, A., 2015. Pipeline free-span observations on Mobile seabeds. In: The 25th International Ocean and Polar Engineering Conference, Kona, Hawaii, USA. In: http://onepetro.org/ISOPEIOPEC/proceedings-pdf/ISOPE15/All-ISOPE15/ISOPE-I-15-513/1335147/isope-i-15-513.pdf.

Matthieu, J., Raaijmakers, T., 2013. Interaction between offshore pipelines and migrating sand waves. In: Proceedings of the International Conference on Offshore Mechanics and Arctic Engineering - OMAE, vol. 4, pp. 203–209. https://doi.org/10.1115/OMAE2012-83875.

Mohr, H., Draper, S., Cheng, L., White, D.J., 2016. Predicting the rate of scour beneath subsea pipelines in marine sediments under steady flow conditions. Coast. Eng. 110, 111–126. https://doi.org/10.1016/J.COASTALENG.2015.12.010.

Palmer, A., 1996. A flaw in the conventional approach to stability design of pipelines. OFFSHORE PIPELINE TECHNOLOGY-CONFERENCE-, pp. 1–10.

Peek, R., Kristiansen, N., 2009. Zero-radius Bend method to trigger lateral buckles. J. Transport. Eng. 135 (12), 946–952. https://doi.org/10.1061/(ASCE)TE.1943-5436.0000076.

Randolph, M.F., White, D.J., 2008a. Offshore foundation design - a moving target: keynote paper. Proceedings of the Second British Geotechnical Association International Conference on Foundations (ICOF).

Randolph, M.F., White, D.J., 2008b. Pipeline embedment in deep water: processes and quantitative assessment. OTC, 19128-MS. https://doi.org/10.4043/otc-19128-ms, 1-16.

Roetert, T., Raaijmakers, T., Borsje, B., 2017. Cable route optimization for offshore wind farms in morphodynamic areas. The 27th International Ocean and Polar Engineering Conference. San Francisco, California, USA. https://onepetro.org/ISOPEIOPEC/proceedings/ISOPE17/All-ISOPE17/ISOPE-I-17-469/18120.

Rodriguez, A.B., Draper, S., Boylan, N.P., Begaj, L., Bransby, M.F., 2014. Pipe soil interaction during cyclic buckling: the importance of site-specific seabed properties. In: Proceedings of the International Conference on Offshore Mechanics and Arctic Engineering - OMAE, 6B. https://doi.org/10.1115/OMAE2014-24391.

Schafer, R.W., 2011. What is a savitzky-golay filter? IEEE Signal Process. Mag. 28 (4), 111–117. https://doi.org/10.1109/MSP.2011.941097.

Soulsby, R.L., Whitehouse, R.J.S., 1997. Threshold of sediment motion in coastal environments. In: Australasian Port and Harbour Conference, pp. 145–150. https://doi.org/10.3316/INFORMIT.929741720399033, 6th : 1997 : Christchurch, *N.Z.*.

Sumer, B.M., Fredsøe, J., 1994. Self-burial of pipelines at span shoulders. Int. J. Offshore Polar Eng. 4 (1). https://onepetro.org/IJOPE/article/26868/Self-Burial-Of-Pipelines-At-Span-Shoulders.

Sumer, B.M., Fredsøe, J., 2002. The mechanics of scour in the marine environment. WORLD SCIENTIFIC. https://doi.org/10.1142/4942.

Sumer, B.M., Truelsen, C., Sichmann, T., Fredsøe, J., 2001. Onset of scour below pipelines and self-burial. Coast. Eng. 42 (4), 313–335. https://doi.org/10.1016/S0378-3839(00)00066-1.

Taner, Y., Hou, Z., Bransby, F., Watson, P., Low, H.E., 2024. Exploring the use of field data to improve predictions of pipeline As-Laid embedment. In: Proceedings of the ASME 2024 43rd International Conference on Ocean, Offshore and Arctic Engineering. Volume 3: Materials Technology; Subsea Technology. ASME, Singapore, Singapore. https://doi.org/10.1115/OMAE2024-123946. V003T04A037.

Unsworth, C.A., Austin, M.J., van Landeghem, K.J.J., Couldrey, A.J., Whitehouse, R.J.S., Lincoln, B., Doole, S., Worrall, P., 2023. Field measurements of cable self-burial in a sandy marine environment. Coast. Eng., 104309 https://doi.org/10.1016/J.COASTALENG.2023.104309.

Van den Abeele, F., Denis, R., 2012. Numerical modelling and analysis for offshore pipeline design, installation, and operation. Journal of Pipeline Engineering 11 (4).

Watson, P.G., Bransby, M.F., Delimi, Z.L., Erbrich, C., Randolph, M.F., Rattley, M., Silva, M., Stevens, B., Thomas, S., Westgate, Z.J., 2019. Foundation design in offshore carbonate sediments–building on knowledge to address future challenges. In: From Research to Applied Geotechnics: Invited Lectures of the XVI Pan-American Conference on Soil Mechanics and Geotechnical Engineering (XVI PCSMGE), p. 240, 17-20 November 2019, Cancun, Mexico, 7.

Westgate, Z.J., White, D.J., Randolph, M.F., 2009. Video observations of dynamic embedment during pipelaying in soft clay. In: Proceedings of the International Conference on Offshore Mechanics and Arctic Engineering - OMAE, pp. 699–707. https://doi.org/10.1115/OMAE2009-79814. *Paper OMAE2009-79814*.

Westgate, Z.J., White, D.J., Randolph, M.F., Brunning, P., 2010. Pipeline laying and embedment in soft fine-grained soils: field observations and numerical simulations. In: Proc. Offshore Technol. Conf.. https://doi.org/10.4043/20407-MS. *Paper OTC 20407*.

Westgate, Z.J., White, D.J., Randolph, M.F., 2012. Field observations of as-laid pipeline embedment in carbonate sediments. Geotechnique 62 (9), 787–798. https://doi.org/10.1680/geot.12.OG.001.

Westgate, Z.J., White, D.J., Randolph, M.F., 2013. Modelling the embedment process during offshore pipe-laying on fine-grained soils. Can. Geotech. J. 50 (1), 15–27. https://doi.org/10.1139/CGJ-2012-0185.

White, D.J., Westgate, Z.J., Tian, Y.H., 2014. Pipeline lateral buckling: realistic modelling of geotechnical variability and uncertainty. In: Proc. Offshore Technol. Conf., vol. 3, pp. 2183–2204. https://doi.org/10.4043/25286-MS. *Paper OTC 25286*.

White, D.J., Westgate, Z.J., Ballard, J.C., De Brier, C., Bransby, M.F., 2015a. Best practice geotechnicai characterization and pipe-soil interaction analysis for HPHT pipeline design. In: Proceedings of the Annual Offshore Technology Conference, vol. 6, pp. 4235–4258. https://doi.org/10.4043/26026-ms.

White, D.J., Leckie, S.H.F., Draper, S., Zakarian, E., 2015b. Temporal changes in pipeline-seabed condition, and their effect on operating behaviour. In: ASME 2015 34th International Conference on Ocean, Offshore and Arctic Engineering. https://doi.org/10.1115/OMAE2015-42216. *Paper OMAE2015-42216*.

Zhang, B.C., An, H.W., Draper, S., Jiang, H.Y., Cheng, L., 2023. Numerical simulations of three-dimensional scour below subsea pipelines/cables under steady current conditions. In: Proceedings of the International Conference on Offshore Mechanics and Arctic Engineering - OMAE, vol. 7. https://doi.org/10.1115/OMAE2023-104579.

Zhang, J.G., Stewart, D.P., Randolph, M.F., 2001. Centrifuge modelling of drained behaviour for pipelines shallowly embedded in calcareous sand. Int. J. Phys. Model. Geotech. 1 (1), 25–39. https://doi.org/10.1680/ijpmg.2001.010104.

Zhang, J.G., Stewart, D.P., Randolph, M.F., 2002. Modeling of shallowly embedded offshore pipelines in calcareous sand. J. Geotech. Geoenviron. Eng. 128 (5), 363–371. https://doi.org/10.1061/(ASCE)1090-0241(2002)128:5(363. ASCE.